*J*ournal of *A*pplied *F*luid *M*echanics, Vol. 9, No. 1, pp. 233-241, 2016.
Available online at www.jafmonline.net, ISSN 1735-3572, EISSN 1735-3645.
DOI: 10.18869/acadpub.jafm.68.224.24052

Unsteady Compressible Flow Calculations with Least-Square Mesh-less Method

S. Sattarzadeh[1], A. Jahangirian[1†] and M.Y. Hashemi[2]

[1]*Department of Aerospace Engineering, Amirkabir University of Technology, Tehran, Iran*
[2]*Department of Mechanical Eng., Azarbaijan Shahid Madani University, Tabriz, Iran*

†*Corresponding Author Email: ajahan@aut.ac.ir*

(Received September 12, 2014; accepted December 28, 2014)

ABSTRACT

A dual-time implicit mesh-less method is presented for unsteady compressible flow calculations. Polynomial least-square (PLS) and Taylor series least-square (TLS) procedures are used to estimate the spatial derivatives at each node and their computational efficiencies are compared. Also, the effect of the neighbor stencil selection on the accuracy of the method is investigated. As a new approach, different neighboring stencils are used for the highly stretched point distribution inside the boundary layer region and the inviscid isotropic point distribution outside this area. The unsteady flows over stationary and moving objects at subsonic and transonic flow conditions are solved. Results indicate the computational efficiency of the method in comparison with the alternative approaches. The convergence histories of the flow solution show that the PLS method is computationally faster than TLS method. In addition, the eight point neighboring stencil inside the viscous region is more efficient than other choices.

Keywords: Navier-Stokes equations; Unsteady compressible flow; Mesh less method; Moving boundary; Implicit method.

NOMENCLATURE

a_{ij}	taylor least square coefficient in x direction
a_i	polynomial least square coefficient
b_{ij}	taylor least square coefficient in y direction
c	chord length
D	artificial dissipation
d_{ij}	distance between point i and j
E	total energy
h	plunging motion
$\bar{h}$	dimensionless form of h
k	reduced frequency
m	mass of the airfoil
M_∞	Mach number in far field
P	pressure
q	heat flux component
r_{ij}	distance between point i and j
$r_{\max}$	the maximum distance between point i and its neighbors
Re_∞	Reynolds number in far field
$\vec{s}_{ij}$	unit vector between i and j
u	velocity component in x direction
U	relative velocity in x direction
U_∞	free-stream velocity
u_n	normal velocity
u_t	tangential velocity
V	relative velocity in y direction
V_n	nodal velocity
w_s	point velocity
x_t	nodal velocity in x direction
y_t	nodal velocity in y direction
v	velocity component in y direction
v_{ij}	pressure sensor at any edges (ij)
$\varepsilon^{(2)}$, $\varepsilon^{(4)}$	local adaptive coefficients
ω_i	weighting factor
α	pitching angle
α_m	mean angle
α_0	oscillation amplitude
ω	frequency of the system
γ	ratio of the specific heats
ρ	density
τ_{xx}	viscous stress terms in x direction
τ	fictitious pseudo-time
$\overline{\nabla\varphi}_{j+1/2}$	the average of gradients of any variable at midpoint

1. INTRODUCTION

One of the main objectives in Computational Fluid Dynamics (CFD) is to solve the numerical computation of flows with complex stationary and/or moving boundaries by using Euler and Navier-Stokes equations. To achieve this goal the quality of the mesh is crucial. Lohner has shown that generating a point cloud distribution which can be applied in mesh-less methods is obviously faster than generating the unstructured grid which is usually used in mesh-based methods (Lohner, *et al.* 2004). It is usually accepted that mesh-less methods are more advantageous in comparison with the mesh based algorithms; especially in the moving and large deformations.

The reason is that replacing and moving points are much simpler than changing or replacing the edges and volumes. Another attractive property of mesh-less methods is the ability of adding or subtracting nodes from the pre-existing nodes. Several mesh-less methods have been used (Liu and Gu 2005; Nguyen *et al.* 2008; Ding *et al* 2004; Deshpande *et al.* 2002; Batina 2003) with different privileges and drawbacks. In these methods, the approximation of the characteristics or derivatives is based on a group of nodes which can be nominated as neighbors. Mesh-less methods need more nodes in comparison with the finite difference method to achieve the same order of accuracy. As a result, the Navier-Stokes equations are solved by great bandwidth of the matrix in these methods. Therefore, the computational memory is unavoidably extensive (Ding *et al.* 2004). In most mesh-less methods explicit time discretizations have been used for solution of the steady-state problems (Deshpande *et al.* 2002; Batina 2003). In the works by Hashemi and Jahangirian (2011) and Sattarzadeh and Jahangirian (2012) an implicit method was presented and it was shown that the method has better convergence behavior in comparison with the similar finite volume (FV) method. One of the main objectives of the present study is to extend the applicability of these mesh-less methods to unsteady flows.

As it is mentioned, the spatial derivatives at each node are normally computed by using least square method. Different approaches are used for this purpose including: Liu and Gu 2005; Ding *et al* 2004; Deshpande *et al.* 2002; Batina 2003; Hashemi and Jahangirian 2011; Katz and Jameson 2009. In this paper, two methods of polynomial least-square (PLS) and Taylor series least-square (TLS) are used and their results are compared in terms of accuracy and computational time in different cases.

The other interested subject is to investigate the effect of neighboring stencils in the efficiency of the computations. In a new attempt different neighboring stencils are used inside and outside the viscous layer in this paper.

2. GOVERNING FLOW EQUATIONS

Navier-Stokes equations that govern the two-dimensional motion of a viscous flow including point movements are:

$$\left[\frac{\partial \mathbf{w}}{\partial t}+\mathbf{w}\nabla \bullet \mathbf{w}_s\right]+\left[\frac{\partial \mathbf{f}^I}{\partial x}+\frac{\partial \mathbf{g}^I}{\partial y}\right]= \frac{\mathrm{M}_\infty}{\mathrm{Re}_\infty}\left[\frac{\partial \mathbf{f}^V}{\partial x}+\frac{\partial \mathbf{g}^V}{\partial y}\right] \quad (1)$$

Here:

$$\mathbf{w}=\begin{pmatrix}\rho\\ \rho u\\ \rho v\\ \rho E\end{pmatrix},\quad \mathbf{w}_s=\begin{pmatrix}x_t\\ y_t\end{pmatrix},$$

$$\mathbf{f}^I=\begin{pmatrix}\rho U\\ \rho uU+P\\ \rho vU\\ \rho EU+Pu\end{pmatrix},\quad \mathbf{g}^I=\begin{pmatrix}\rho V\\ \rho uV\\ \rho vV+P\\ \rho EV+Pv\end{pmatrix}$$

$$\mathbf{f}^V=\begin{pmatrix}0\\ \tau_{xx}\\ \tau_{xy}\\ u\tau_{xx}+v\tau_{xy}-q_x\end{pmatrix},\mathbf{g}^V=\begin{pmatrix}0\\ \tau_{xy}\\ \tau_{yy}\\ u\tau_{xy}+v\tau_{yy}-q_y\end{pmatrix} \quad (2)$$

The superscripts *I* and *V* shows the inviscid and viscous terms (Hashemi and Jahangirian 2011). In this equation, the velocities (U and V) can be evaluated as:

$$U=u-x_t\ ,\ V=v-y_t \quad (3)$$

For a perfect gas (Sattarzadeh and Jahangirian 2012):

$$p=(\gamma-1)\rho\left[E-\frac{u^2+v^2}{2}\right] \quad (4)$$

3. LEAST-SQUARE MESH-LESS METHOD

3.1 Taylor Series Least-Square Method

In this paper, the equations are solved in the conservation form and the least-square mesh-less algorithm is applied (Sattarzadeh and Jahangirian 2012). It is considered that C_i is a group of points that are neighbors to point *i* (Fig. 1) and ϕ_{ij} is a value of any function ϕ at the mid-point of each pair point *ij* (Katz and Jameson 2009). By using Taylor's formula for *i* and its neighbor (*j*) one can have:

$$\left(\frac{\partial \phi}{\partial x}\right)_i \Delta x_{ij}+\left(\frac{\partial \phi}{\partial y}\right)_i \Delta y_{ij}=\Delta\phi_{ij} \quad (5)$$
$$\Delta x_{ij}=x_j-x_i\ ,\ \Delta y_{ij}=y_j-y_i\ ,\ \Delta\phi_{ij}=\phi_j-\phi_i$$

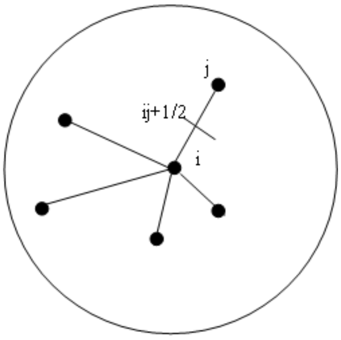

Fig. 1. Schematic of point and its neighbors.

Similar equations could be written for all neighbors related to the point *i* by considering an arbitrary weighting factor. Thus, the following matrix can be achieved (Hashemi and Jahangirian 2011; Sattarzadeh and Jahangirian 2012):

$$\begin{bmatrix} \omega_{i1}\Delta x_{i1} & \omega_{i1}\Delta y_{i1} \\ ..... & ..... \\ \omega_{im}\Delta x_{im} & \omega_{im}\Delta y_{im} \end{bmatrix} \begin{bmatrix} \left.\dfrac{\partial\phi}{\partial x}\right|_i \\ \left.\dfrac{\partial\phi}{\partial y}\right|_i \end{bmatrix} = \begin{bmatrix} \omega_{i1}\Delta\phi_{i1} \\ ...... \\ \omega_{im}\Delta\phi_{im} \end{bmatrix} \tag{6}$$

Where weighting factor is chosen as the inverse distance between points *i* and *j*. By using the Taylor least-squares method in Eq. (6) the derivatives can be achieved as follows (Sattarzadeh and Jahangirian 2012):

$$\left.\frac{\partial\phi}{\partial x}\right|_i = \sum_{j=1}^{m} a_{ij}\,\Delta\phi_{ij} \quad , \quad \left.\frac{\partial\phi}{\partial y}\right|_i = \sum_{j=1}^{m} b_{ij}\,\Delta\phi_{ij} \tag{7}$$

By counting weighting function, the coefficients in Eq. (7) can be calculated as (Hashemi and Jahangirian 2011; Katz and Jameson 2009; Luo *et al.* 2009):

$$a_{ij} = \frac{\omega_{ij}\Delta x_{ij}\sum_{k=1}^{m}\omega_{ik}\Delta y_{ik}{}^{2} - \omega_{ij}\Delta y_{ij}\sum_{k=1}^{m}\omega_{ik}\Delta x_{ik}\Delta y_{ik}}{\sum_{k=1}^{m}\omega_{ik}\Delta x_{ij}{}^{2}\sum_{k=1}^{m}\omega_{ik}\Delta y_{ik}{}^{2} - \left(\sum_{k=1}^{m}\omega_{ik}\Delta x_{ik}\Delta y_{ik}\right)^{2}}$$

$$b_{ij} = \frac{\omega_{ij}\Delta y_{ij}\sum_{k=1}^{m}\omega_{ik}\Delta x_{ik}{}^{2} - \omega_{ij}\Delta x_{ij}\sum_{k=1}^{m}\omega_{ik}\Delta x_{ik}\Delta y_{ik}}{\sum_{k=1}^{m}\omega_{ik}\Delta x_{ij}{}^{2}\sum_{k=1}^{m}\omega_{ik}\Delta y_{ik}{}^{2} - \left(\sum_{k=1}^{m}\omega_{ik}\Delta x_{ik}\Delta y_{ik}\right)^{2}} \tag{8}$$

3.2 Polynomial Series Least-Square Method

Another way to obtain derivatives is the polynomial least square method. The major difference between PLS and TLS is that in PLS method, the computed polynomial is not forced to pass the point while the Taylor approximation always pass the point. In this method, a polynomial basis function is used as following (Katz and Jameson 2009):

$$\phi_{ij} = a_1 + a_2 x + a_3 y \tag{9}$$

By considering the least square method and minimizing the following equation with regard to Polynomial least square coefficient (Hashemi and Jahangirian 2011):

$$\sum_{j=1}^{n}\omega_{ij}\left[\phi_{ij} - a_1 - a_2 x_{ij} - a_3 y_{ij}\right]^2 \tag{10}$$

Using normalized Gaussian function, the weight function can then be calculated as:

$$\omega_{ij} = \frac{e^{-(\frac{r_{ij}}{r_{\max}})^2} - e^{-4}}{1 - e^{-4}} \tag{11}$$

By solving Eq. (10) for each node the Polynomial least square coefficient can be calculated (Hashemi and Jahangirian 2011). Then, the derivatives for parameter ϕ at point *i* can be achieved as following:

$$\left.\frac{\partial\phi}{\partial x}\right|_i = a_{2i} \quad , \quad \left.\frac{\partial\phi}{\partial y}\right|_i = a_{3i} \tag{12}$$

4. NUMERICAL IMPLEMENTATION

After defining the least-square coefficient the semi-discrete form of the Navier-Stokes equations at point *i* is presented as following:

$$\left[\frac{\partial \mathbf{w}_i}{\partial t} + \mathbf{w}_i\left(\sum_{j=1}^{m} a_{ij}\Delta x_{t,ij} + \sum_{j=1}^{m} b_{ij}\Delta y_{t,ij}\right)\right] + \left[\sum_{j=1}^{m} a_{ij}\Delta\mathbf{f}_{ij}^{I} + \sum_{j=1}^{m} b_{ij}\Delta\mathbf{g}_{ij}^{I}\right] = \frac{\mathrm{M}_\infty}{\mathrm{Re}_\infty}\left[\sum_{j=1}^{m} a_{ij}\Delta\mathbf{f}_{ij}^{V} + \sum_{j=1}^{m} b_{ij}\Delta\mathbf{g}_{ij}^{V}\right] \tag{13}$$

Here $\Delta\mathbf{f}_{ij} = \mathbf{f}_j - \mathbf{f}_i$ and $\Delta g_{ij} = g_j - g_i$. Then, a flux $H = af + bg$ for each pair points such as *ij* is defined which is similar to flux calculation on mesh-base methods. So the Eq. (13) with the direct flux becomes (Hashemi and Jahangirian 2011):

$$\left(\frac{\partial \mathbf{w}_i}{\partial t} + \mathbf{w}_i\left(\sum_{j=1}^{m} a_{ij}\Delta x_{t,ij} + \sum_{j=1}^{m} b_{ij}\Delta y_{t,ij}\right)\right) + \sum_{j=1}^{m}\Delta\mathbf{H}_{ij}^{I} = \frac{\mathrm{M}_\infty}{\mathrm{Re}_\infty}\left[\sum_{j=1}^{m}\Delta\mathbf{H}_{ij}^{V}\right] \;,\; \Delta\mathbf{H}_{ij} = \mathbf{H}_j - \mathbf{H}_i \tag{14}$$

It is proved that the discretization will be stable, if for any cloud point; the local Reynolds number is less than two. To assure this limitation, one way is to increase the number of points in the domain which is unnecessary and may lead to low computational efficiency. Another way to stabilize the method is to use artificial dissipation. In the present study, artificial dissipation is added in order to diminish the oscillations (Swanson *et al.* 1998):

$$\left(\frac{\partial \mathbf{w}_i}{\partial t} + \mathbf{w}_i\left(\sum_{j=1}^{m} a_{ij}\Delta x_{t,ij} + \sum_{j=1}^{m} b_{ij}\Delta y_{t,ij}\right)\right) + 2\sum_{j=1}^{m}\Delta\mathbf{H}_{ij+1/2}^{I} - \frac{2\mathrm{M}_\infty}{\mathrm{Re}_\infty}\left[\sum_{j=1}^{m}\Delta\mathbf{H}_{ij+1/2}^{V}\right] - D_i = 0 \tag{15}$$

Where D_i is dissipation term. In this investigation the JST method described in Hashemi and Jahangirian 2011 is used.

By using Eq. (15) for all points in the domain, the following equations are achieved (Hashemi and Jahangirian 2011):

$$\frac{\partial \mathbf{w}_i}{\partial t} + \mathbf{R}_i\left(\mathbf{w}\right) = 0 \tag{16}$$

Where:

$$\begin{aligned}\mathbf{R}_i\left(\mathbf{w}\ \right) = \mathbf{w}_i &\left(\sum_{j=1}^{m} a_{ij}\Delta x_{t,ij} + \sum_{j=1}^{m} b_{ij}\Delta y_{t,ij} \right) \\ &+2\sum_{j=1}^{m} \Delta\mathbf{H}_{ij+1/2}^{I}\left(\mathbf{w}\ \right) \\ &-2\frac{\mathrm{M}_\infty}{\mathrm{Re}_\infty}\left[\sum_{j=1}^{m} \Delta\mathbf{H}_{ij+1/2}^{V}\left(\mathbf{w}\ \right)\right] - \mathbf{D}_i\end{aligned} \tag{17}$$

The discretization of the first term in Eq. (16) can be achieved by different methods such as explicit or implicit methods which are explained in the next section.

4.1 Time Integration

explicit time integration

In the present study, the explicit four-stage Runge-Kutta (R-K) scheme is used. Local time stepping at each node can be calculated by using its neighbor nodes. To increase the computational efficiency, the dissipation function is calculated only at the first and third stages. These values are then used for the subsequent second and fourth stages. Further details can be obtained from references (Hashemi and Jahangirian 2011; Sattarzadeh and Jahangirian 2012).

implicit time integration

In the implicit method, the solution involves the current and later time. By applying a fully implicit time method, the flow Eq. (14) is integrated in time as follows (Jahangirian and Hadidoolabi, 2005):

$$\frac{\partial \mathbf{w}_i^{n+1}}{\partial t} + \mathbf{R}_i\left(\mathbf{w}^{n+1}\right) = 0 \tag{18}$$

A second order accurate time discretization is used in the present study (Hashemi and Jahangirian 2011; Jahangirian and Hadidoolabi 2005). So, the Eq. (18) can be rewritten as follows:

$$\frac{3\mathbf{w}_i^{n+1}}{2\Delta t_i} - \frac{4\mathbf{w}_i^{n}}{2\Delta t_i} + \frac{\mathbf{w}_i^{n-1}}{2\Delta t_i} + \mathbf{R}_i\left(\mathbf{w}^{n+1}\right) = 0 \tag{19}$$

Since Eq. (19) is nonlinear for parameter $\mathbf{w}_i^{n+1}$ and so it cannot be solved analytically. To overcome this problem, a new residual is useful to redefine at this stage, which is equal to the left side of Eq. (19):

$$\begin{aligned}\mathbf{R}_i^*\left(\mathbf{w}^{n+1}\right) = &\frac{3\mathbf{w}_i^{n+1}}{2\Delta t_i} - \frac{4\mathbf{w}_i^{n}}{2\Delta t_i} + \frac{\mathbf{w}_i^{n-1}}{2\Delta t_i} \\ &+ \mathbf{w}_i^{n+1}\left(\sum_{j=1}^{m} a_{ij}\Delta x_{t,ij} + \sum_{j=1}^{m} b_{ij}\Delta y_{t,ij} \right) \\ &+ \sum_{j=1}^{m} \Delta\mathbf{H}_{ij}^{I}\left(\mathbf{w}^{n+1}\right) \\ &- \frac{\mathrm{M}_\infty}{\mathrm{Re}_\infty}\left[\sum_{j=1}^{m} \Delta\mathbf{H}_{ij}^{V}\left(\mathbf{w}^{n+1}\right)\right] - \mathbf{D}_i\left(\mathbf{w}^{n+1}\right)\end{aligned} \tag{20}$$

Eq. (20) can be considered as the solution of steady-state and unsteady problems which can be solved with a time marching method as follows (Hashemi and Jahangirian 2011; Sattarzadeh and Jahangirian 2012):

$$\frac{\partial \mathbf{w}_i^{n+1}}{\partial \tau} + \mathbf{R}_i^*\left(\mathbf{w}^{n+1}\right) = 0 \tag{21}$$

The pseudo-time problem can be solved by using a time-marching method such as explicit method. In this paper, Eq. (21) is solved by using the explicit Runge-Kutta scheme (Jahangirian and Hadidoolabi 2005).

The Courant number (CFL) of 2-5 and 100000-500000 is used for explicit and implicit iterations, respectively in this study (Hashemi and Jahangirian 2011).

4.2 Viscous Term

Like the other flux terms, viscous terms are calculated at the middle of each pair point. In these terms the gradients of temperature and velocity components exist and therefore, to calculate the viscous terms, the average of these gradients at the midpoint is needed. In the present study the following equations which are applied in references (Hashemi and Jahangirian 2011; Katz and Jameson 2009; Alonso *et al*. 2005) are used:

$$\nabla\varphi_{j+1/2} = \overline{\nabla\varphi}_{j+1/2} - \left(\overline{\nabla\varphi}_{j+1/2} \bullet \vec{s}_{ij} - \frac{\varphi_j - \varphi_i}{\left\|\vec{L}_{ij}\right\|} \right)\vec{s}_{ij} \tag{22}$$

Here:

$$\overline{\nabla\varphi}_{j+1/2} = \left(\frac{\nabla\varphi_i + \nabla\varphi_j}{2} \right)\ ,\ \vec{s}_{ij} = \left(\frac{\vec{L}_{ij}}{\left\|\vec{L}_{ij}\right\|} \right) \tag{23}$$

Therefore;

$$\begin{aligned}&\tau_{xy,\,j+1/2} = \frac{1}{2}\left(\mu_i^* + \mu_j^*\right) * \\ &\left(\left(\frac{\partial u}{\partial y}\right)_{j+1/2} + \left(\frac{\partial v}{\partial x}\right)_{j+1/2} \right)\end{aligned} \tag{24}$$

To solve equations at solid boundary, it is presumed that mass or other fluxes cannot penetrate to the solid body (Sattarzadeh and Jahangirian 2012; Katz and Jameson 2009). In addition for viscous flow, no-slip boundary condition is used (Hashemi and Jahangirian 2011). To increase the accuracy specially, in the solid region, the Ghost point method is used in this investigation (Hashemi and Jahangirian 2011; Katz and Jameson 2009). To satisfy the far field conditions, the Riemann invariants is applied (Sattarzadeh and Jahangirian 2012; Katz and Jameson 2009; Jahangirian and Hadidoolabi 2005). ysis is theThe drawback of the characteristic anal assumption of zero circulation. To dominate this problem, the far field should be

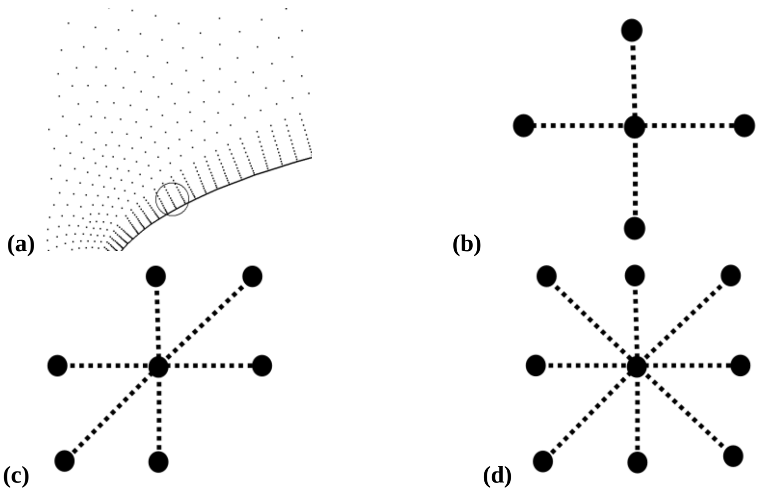

Fig. 2. Different neighbor stencils in viscous region. a) point distribution b) 4 points c) 6 points d) 8 points stencils.

far enough from the solid boundary (Katz and Jameson 2009).

4.3 Neighbor Selection

One of the privileges of mesh-less method in comparison with mesh-based method, is their flexibility in choosing neighbors. In these methods, there is no connection between points so the neighbors of each point can be chosen in different ways without having any special problem. One of the critical zones in solving N-S equations is boundary layer zones which has its complexity in grid generation. Thus, in this paper special care has been taken in order to choose an efficient neighbor stencil for points inside the viscous layer. Three different neighbor stencils are selected and applied in this work that, are shown in Figure 2. As sketched in this figure 4 points, 6 points and 8 points stencils are applied and the results are compared.

Another aspect that applied in this work is the satisfaction of reciprocity condition. This condition means that in mesh-less method when a point (for example i) is chosen as a neighbor for the other point (for example j), the second point (j) is also necessarily a neighbor of the first point (i) (Fig.3a). This has proved to be a more accurate way for calculations.

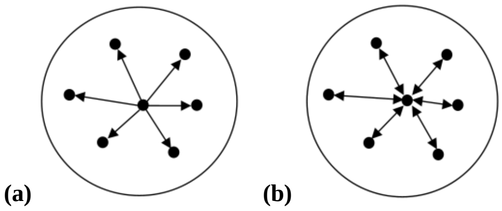

Fig.3. Choosing neighbors for each pair points.

5 RESULTS

The first test case is chosen to show the validity of the method for unsteady flows. A subsonic inviscid flow around NACA0012 airfoil is considered at Mach number 0.5 and angle of attack zero degree. The point distribution is shown in Fig. 4. The domain includes 6509 points in which 280 points are on the solid boundary and 60 points are on the outer boundary.

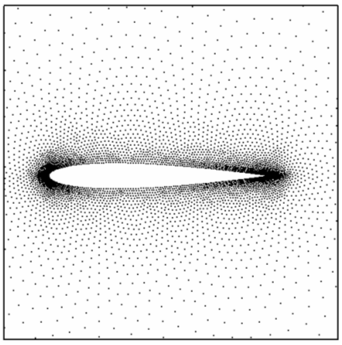

Fig. 4. Point distribution over NACA0012 airfoil (inviscid case).

In this case, explicit CFL number of 5 and implicit CFL number of 100000 are used. The surface pressure coefficient distributions by two different methods (Lagrangian and Eulerian methods) are shown in Fig. 5. As it is seen, the results are in good agreements with AGARD (1982) data, confirming the acceptable accuracy of the present mesh-less method.

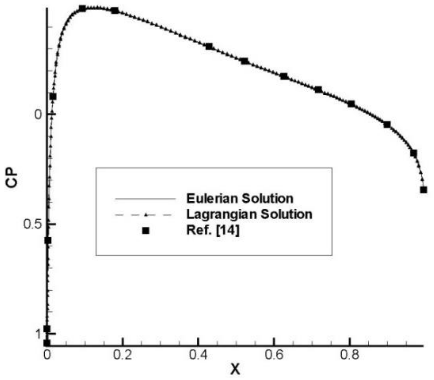

Fig. 5. Surface pressure coefficients at M= 0.5 and AOA= 0.

In this case TLS method is used. The convergence history for this case is shown in Fig.6, which demonstrates the computational efficiency of the implicit mesh-less method in comparison with the explicit approach (Sattarzadeh and Jahangirian 2012).

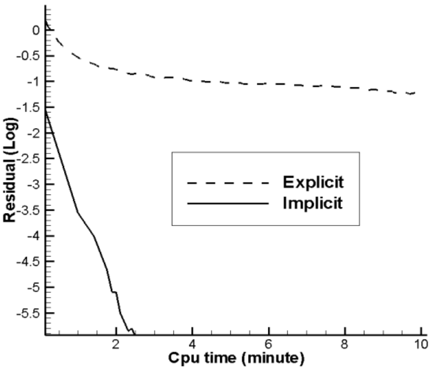

Fig. 6. Convergence history for NACA 0012 airfoil at M =0.5 and AOA= 0.

The second case is defined to show the effect of different neighbor stencils in viscous region. Three different neighboring stencils which are introduced in the previous section (Fig. 3) are applied. The number of neighbors for different choices is four, six and eight. The flow conditions around NACA0012 airfoil for this laminar case are Reynolds number 500, incidence angle 10 degrees and Mach number 0.8. The point distribution around NACA0012 is shown in Fig. 7.

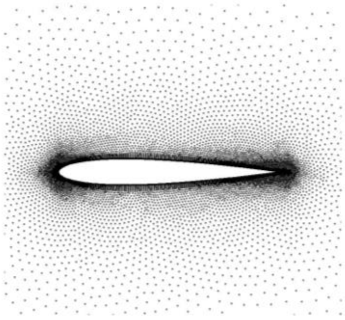

Fig. 7. Point distribution over NACA0012 airfoil (viscous case).

In this case the number of points is 6169 in which 200 points are on the boundary layer, and 126 points are on the outer boundary. Also in this case, the results of Polynomial least square (PLS) and Taylor series least square (TLS) are compared. The surface pressure coefficients for different choices of neighbors using PLS and TLS methods are shown in Fig. 8. According to this figure the main effect due to different neighbor stencils is visible only near the leading edge on the upper surface of the airfoil. The PLS and TLS results are very compatible in this case. The convergence histories for PLS and TLS methods with different neighbor stencils are presented in figures 9. As expected the eight-point stencil has better rate of convergence in comparison with the other two choices. Also, by comparing figures 9(a) and 9(b) the convergence rate in PLS method is better than TLS method. Thus, in the following computations PLS method is used.

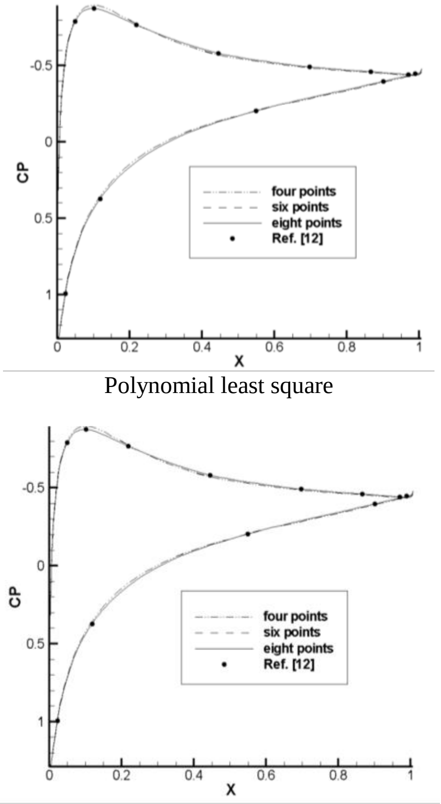

Polynomial least square

Taylor least square

Fig. 8. Surface pressure coefficients at M= 0.8, AOA= 10 and Re=500.

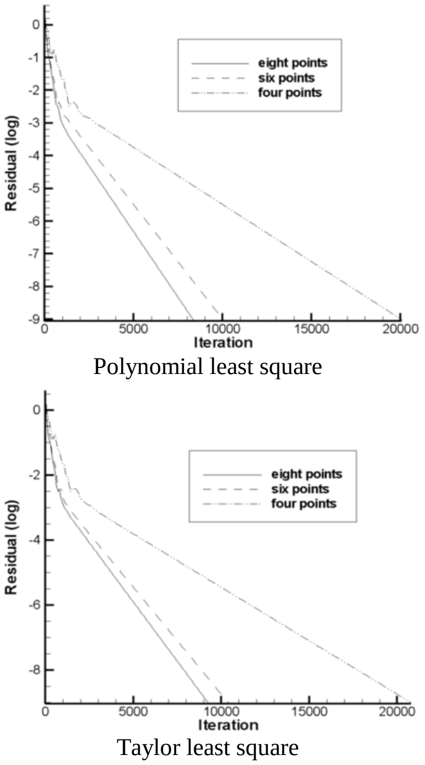

Polynomial least square

Taylor least square

Fig. 9. Convergence history for NACA 0012 airfoil at M =0.8, AOA= 10 and Re=500.

In order to further investigate the computational efficiency of the presented methods the convergence histories are shown against the computational time in figure 10. As it is shown the six and eight points stencils needs 50% less computational time to reach the steady state solution.

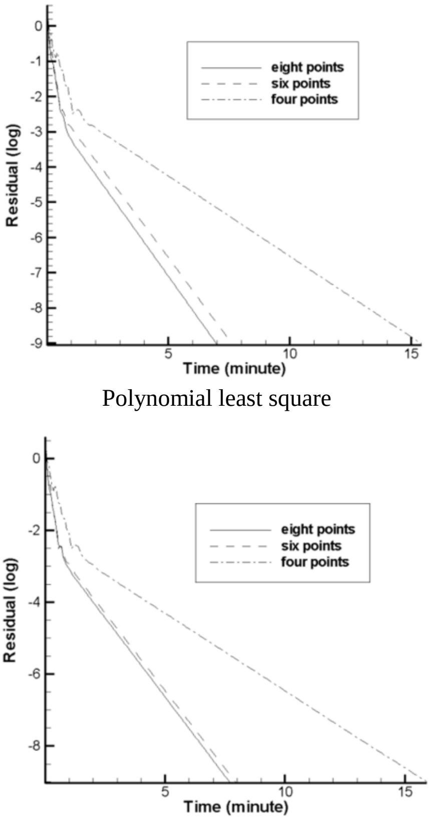

Polynomial least square

Taylor least square

Fig. 10. Convergence history for NACA 0012 airfoil at M =0.8, AOA= 10 and Re=500.

The third test case is defined to show the potential of the presented mesh-less method to simulate the unsteady flow around a circular cylinder. The flow condition for this test case is Re=500 at Mach number 0.2. The flow includes the unsteady vortices that alternatively shed from the body (Karman Vortex Street) and flow downstream. The point distribution is shown in Fig. 11.

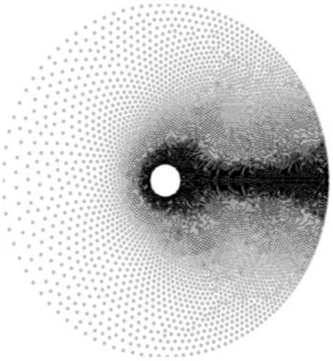

Fig. 11. Point distribution around circular cylinder at Re = 500.

In this test case the eight point neighbors is chosen. There are 12347 points in the domain. The time history of the lift coefficient is shown in Fig. 12 demonstrating the periodic behavior of the flow. The maximum and minimum converged lift coefficients in this case are -1.122 and 1.121 which show less than 1 percent difference with the numerical data reported by Alonso (2005). The pressure contours at different time steps are shown in Fig. 13.

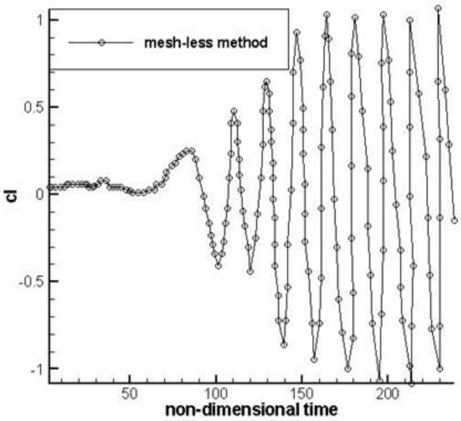

Fig. 12. Time history of the lift coefficient around circular cylinder, Re = 500.

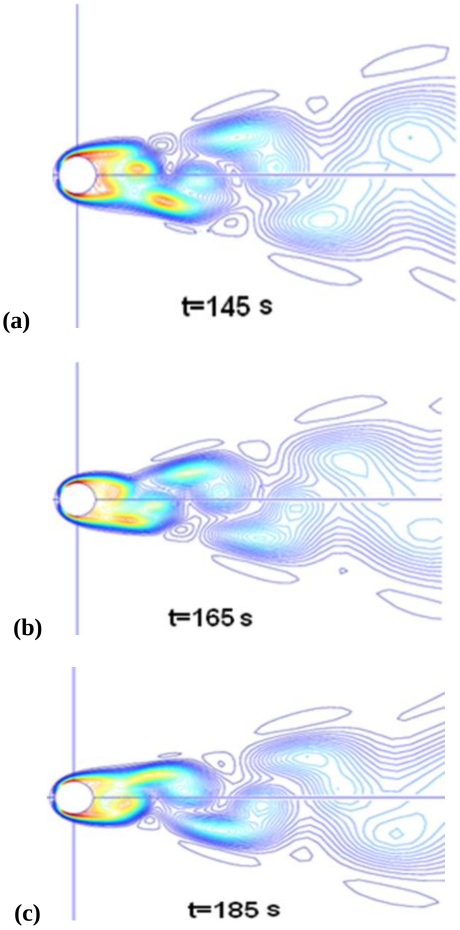

Fig. 13. Pressure contours at three different times, Re = 500.

The next case is an unsteady inviscid flow solution around oscillating NACA0012 airfoil at Mach number of 0.755. The point distribution is the same as the first test study. The points are moved by the movement of the solid boundary and the periodic angle about the quarter chord can be calculated as follows:

$$\alpha(t) = \left(\alpha_m + \alpha_0 \sin(\omega t)\right) \qquad (25)$$

In this equation, the mean angle α_m is chosen as 0.016 and the oscillation amplitude α_0 is taken as 2.51. In this equation the frequency of the system is calculated as:

$$\omega = \frac{2kU_\infty}{c} \qquad (26)$$

In this investigation k is chosen as 0.814. In Fig. 14, the pressure contours of the flow field in different time steps are shown.

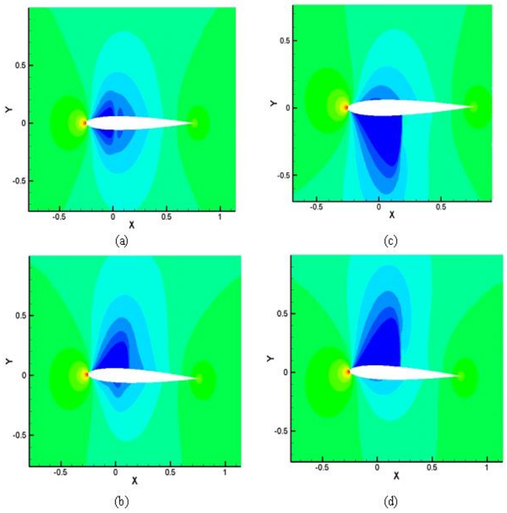

Fig. 14. A few snap shots of the flow field at Mach number of 0.755.

Fig. 15 indicates normal force coefficient and pitching moment coefficients. In these figures, the results of inviscid flow are compared with the experimental data of the AGARD (1982) and Control Volume numerical results from Jahangirian and Hadidoolabi (2005). As illustrated the mesh less results are in good agreement with the finite-volume results.

(a)

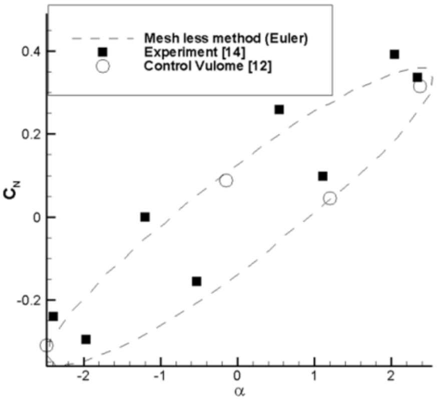

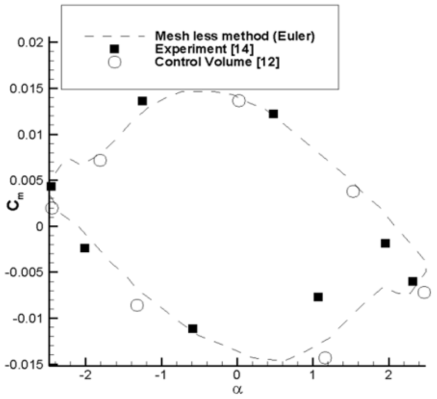

(b)

Fig. 15. (a) Normal force coefficient (b) Pitching moment coefficient at Mach number of 0.755.

6 CONCLUSIONS

In this study, a dual-time implicit mesh-less method for unsteady compressible flows including moving boundaries was presented. To estimate the spatial derivatives at each node, Polynomial and Taylor series least-square methods were used. Three different neighboring stencils are employed in the viscous region and it was concluded that the eight point stencil had better numerical behavior i.e. less computational time. The unsteady flows over stationary and moving objects at subsonic and transonic flow conditions were solved. Results indicated that the method is able to employ for different unsteady flow solutions with the comparable accuracy with the other known finite volume methods. The results also showed that the PLS method had better convergence rate in comparison with TLS method.

REFERENCES

Alonso, J., L. Martinelli and A. Jameson (2005, January). Multigrid Unsteady Navier-stokes Calculations with Aeroelastic Applications. *AIAA 43rd Aerospace Sciences Meeting*, No. 0318, Reno, Nevada.

Batina, J. T. (1993). A gridless Euler/Navier-Stokes solution algorithm for complex aircraft applications. *AIAA Paper* 93.

Compendium of Unsteady Aerodynamic Measurements (1982). AGARD, R- 702.

Deshpande, S. M., C. Praveen and V. Ramesh (2002). Theory and application of 3-D LSKUM based on entropy variables. *International Journal for Numerical Methods in Engineering* 40, 47-62.

Ding, H., C. Shu, K. S. Yeo and D. Xu (2004). Simulation of incompressible viscous flows past a circular cylinder by hybrid FD scheme and mesh-less least square-based finite difference method. *Computer Methods in Applied Mechanics and Engineering* 193, 727-744.

Hashemi, Y. and A. Jahangirian (2011). An efficient implicit mesh-less method for compressible calculations. *International Journal for Numerical Methods in Fluids* 67, 754-770.

Jahangirian, A. and M. Hadidoolabi (2005). Unstructured moving grids for implicit calculation of unsteady compressible viscous flows. *Journal for Numerical Methods in Fluids* 47, 1107-1113.

Katz, A. and A. Jameson (2009, January). A Comparison of Various Meshless Schemes Within a Unified Algorithm. *AIAA Paper 2009-596,* 47th AIAA Aerospace Sciences Meeting including The New Horizons Forum and Aerospace Exposition, Orlando, Florida.

Liu, G. R. and Y. T. Gu (2005). *An introduction to mesh-free methods and their programming*. Springer, The Netherlands.

Lohner, R. and E. Onate (2004). A general advancing front technique for filling space with arbitrary objects. *International Journal for Numerical Methods in Engineering,* 61,1977-1991.

Luo, H., J. D. Baum and R. Lohner (2009). A hybrid building-block and gridless method for compressible flows. *International Journal for Numerical Methods in Fluids* 59, 459-474.

Nguyen, V. P., T. Rabczuk, S. Bordas and M. Marc Duot (2008). Mesh-less methods: A review and computer implementation aspects, *Mathematics and Computers in Simulation* 797,63-813.

Sattarzadeh, S. and A. Jahangirian (2012). 3D Implicit Mesh-less Method for Compressible Flow Calculations. *Scientia Iranica* 19, 503-512.

Swanson, R.C., R. Radespiel and E. Turkel (1998). On Some Numerical Dissipation Schemes. *Journal of computational Physics* 147, 518-544.